Supplementary Information for

Supported Polymeric Organic Framework Composed of Dual Electrocatalytic Active Sites for High-Performance Carbon Dioxide Electroreduction

Shengsheng Huang[a], Qizhe He[a], Hongwei Li[a], Jinjie Qian[b,*], Wei Xu[a], Ting-Ting Li[a,*]

[a]School of Materials Science and Chemical Engineering, Ningbo University, Ningbo, 315211, China.

[b]College of Chemistry and Materials Engineering, Wenzhou University, Wenzhou, 325000, China.

*Corresponding author. E-mail addresses: jinjieqian@wzu.edu.cn (J. Qian), litingting@nbu.edu.cn (T.-T. Li).

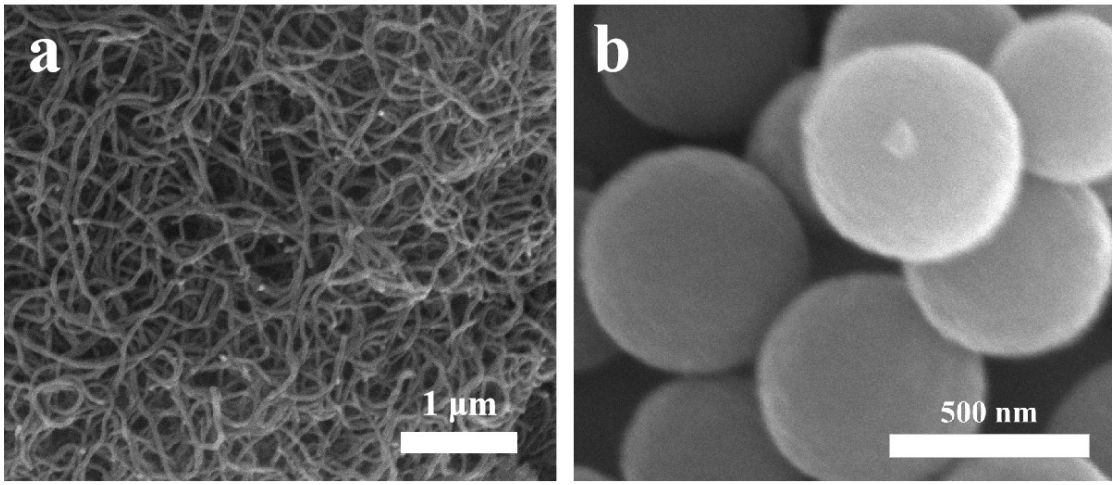

Fig. S1. SEM images of (a) CoPOF-Bpy@CNT and (b) CoPOF-Bpy.

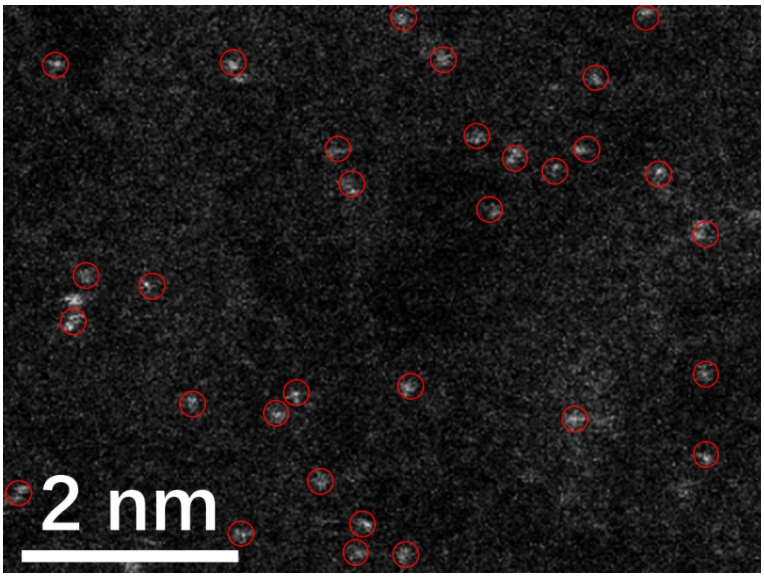

Fig. S2. AC HAADF-STEM image of CoPOF-Bpy@CNT, partial of single Co atoms are highlighted by red circles.

Table S1 The Co contents of the samples.

Sample	Co wt%
CoPOF-Bda@CNT	1.9
CoPOF-Bpda@CNT	1.8
CoPOF-Bpy@CNT	3.7

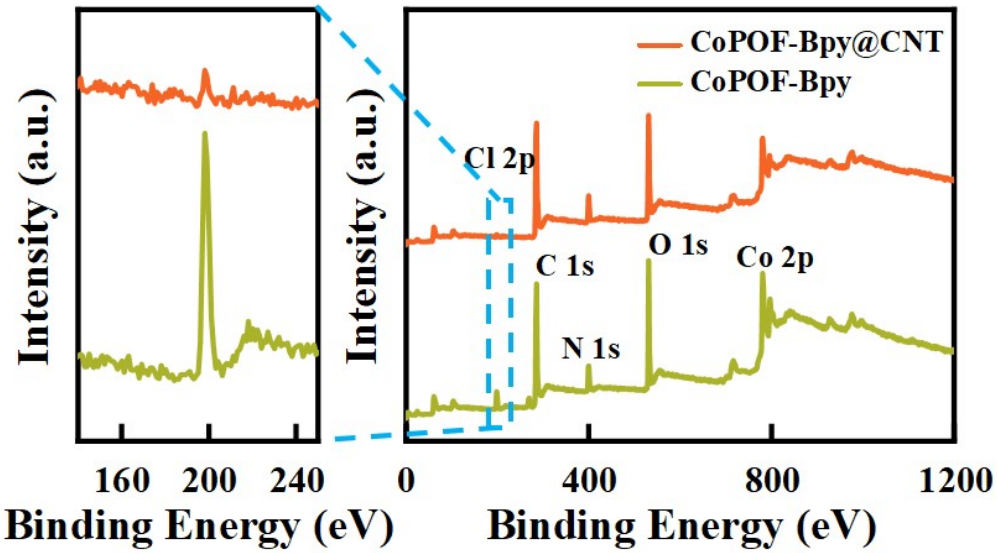

Fig. S3. XPS spectra of CoPOF-Bpy@CNT and CoPOF-Bpy.

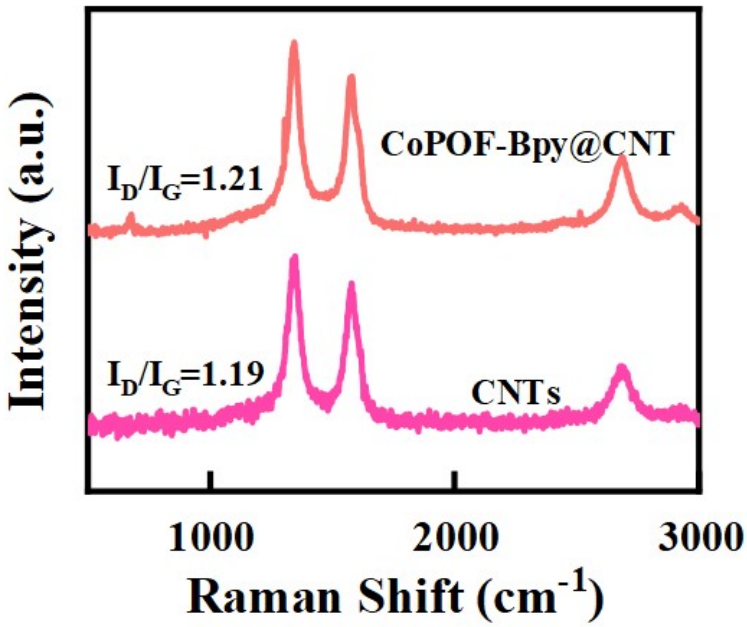

Fig. S4. Raman spectra of CoPOF-Bpy@CNT and CNTs.

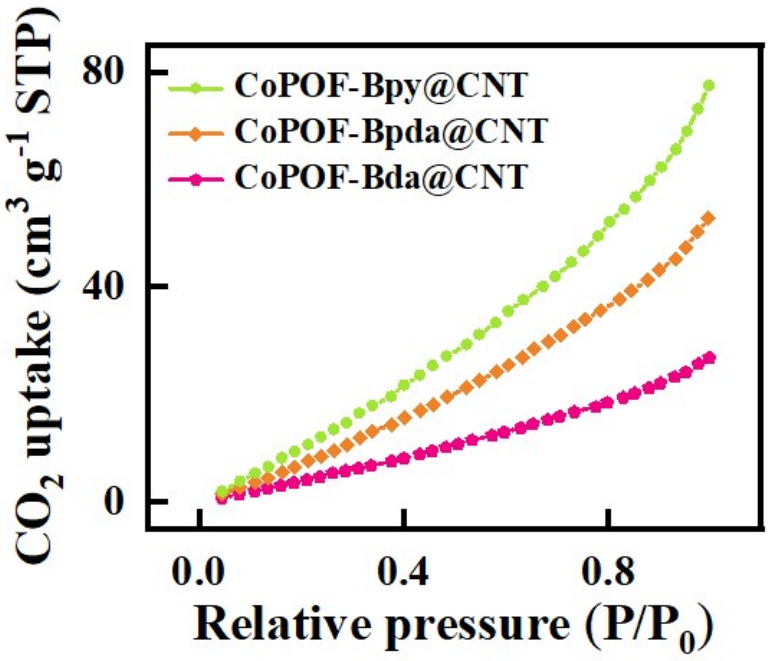

Fig. S5. CO_2 adsorption isotherms of CoPOF-Bpy@CNT, CoPOF-Bpda@CNT, and CoPOF-Bda@CNT at 298 K.

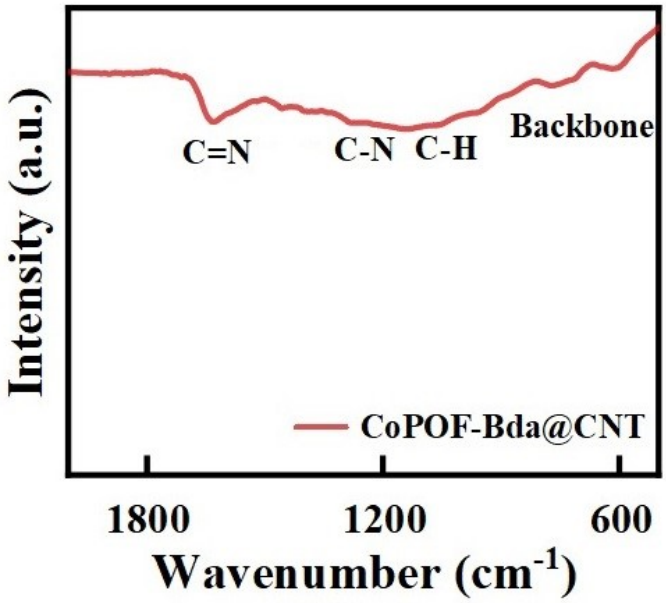

Fig. S6. FT-IR spectrum of CoPOF-Bda@CNT.

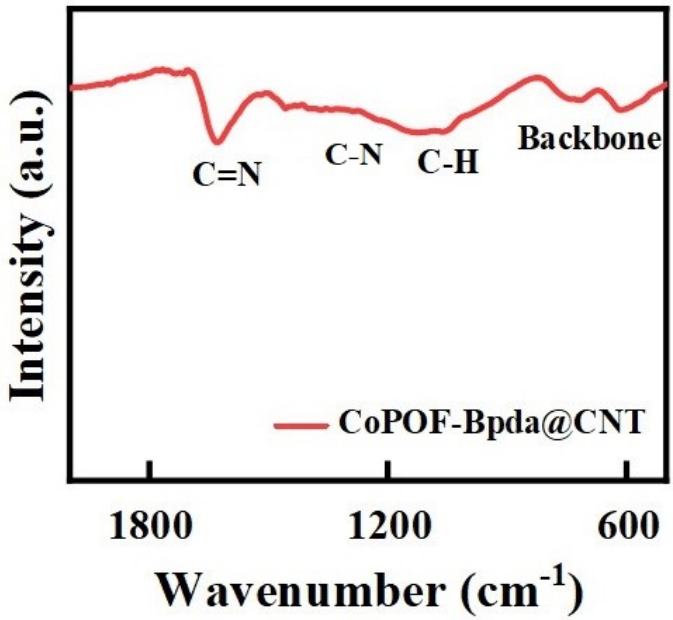

Fig. S7. FT-IR spectrum of CoPOF-Bpda@CNT.

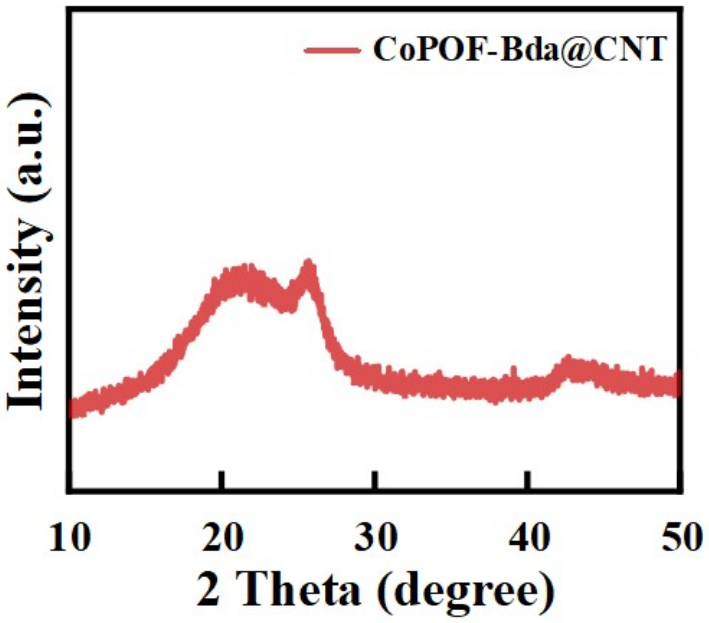

Fig. S8. XRD patterns of CoPOF-Bda@CNT.

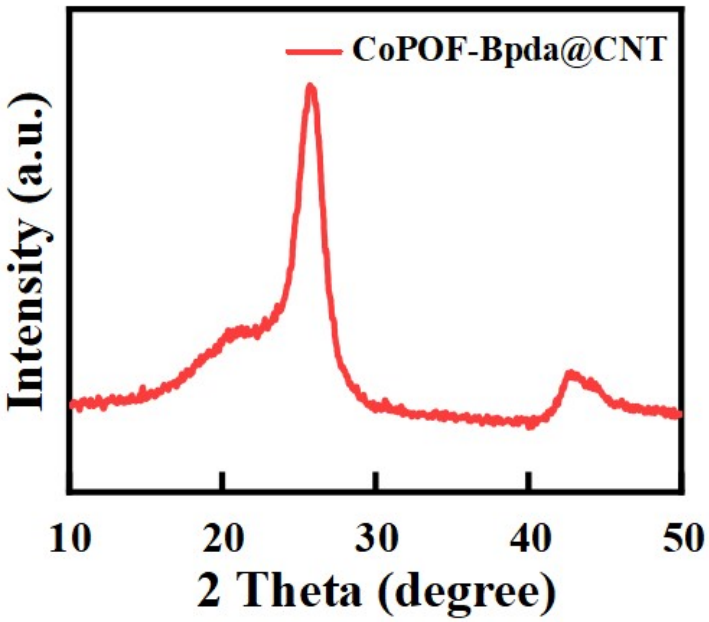

Fig. S9. XRD patterns of CoPOF-Bpda@CNT.

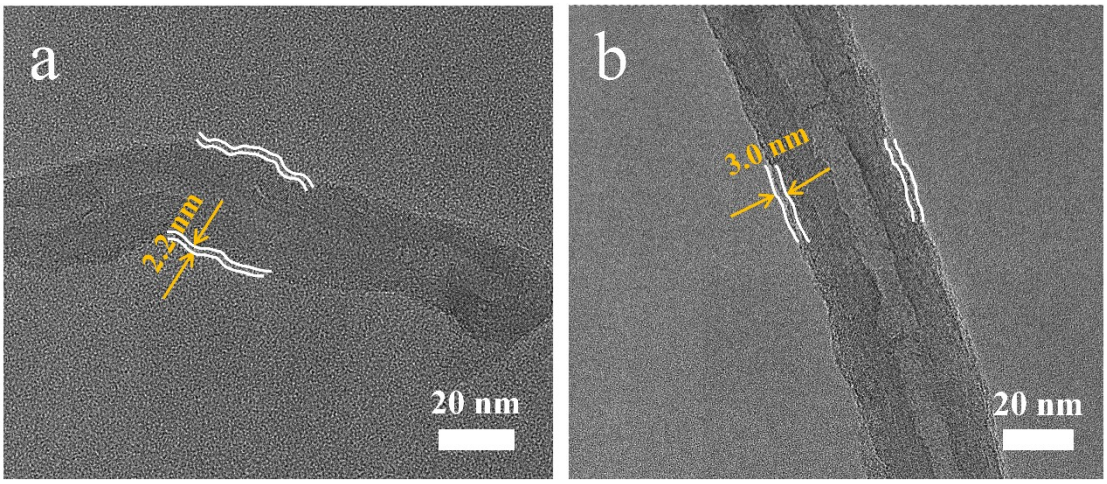

Fig. S10. TEM images of (a) CoPOF-Bda@CNT and (b) CoPOF-Bpda@CNT.

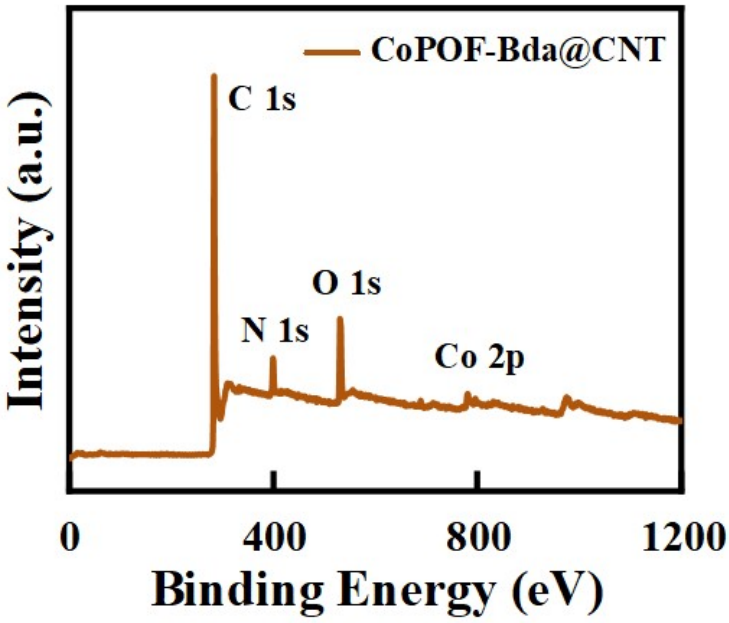

Fig. S11. XPS spectrum of CoPOF-Bda@CNT.

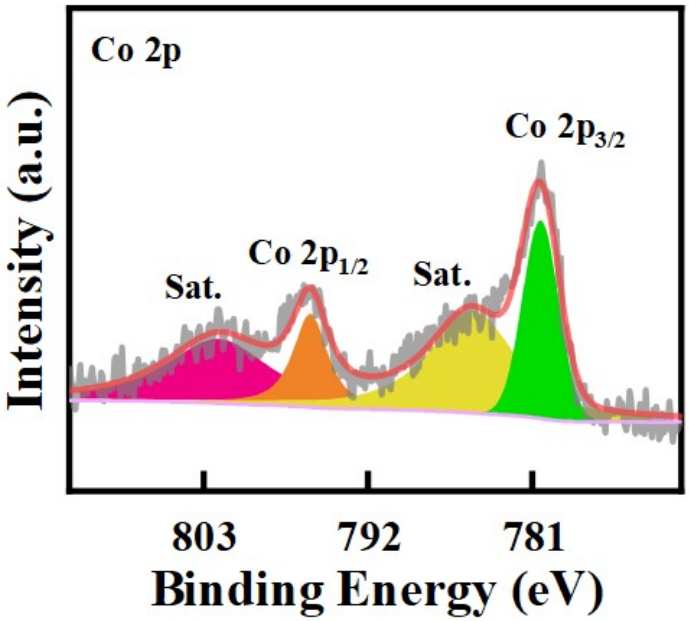

Fig. S12. Co 2p XPS spectrum of CoPOF-Bda@CNT.

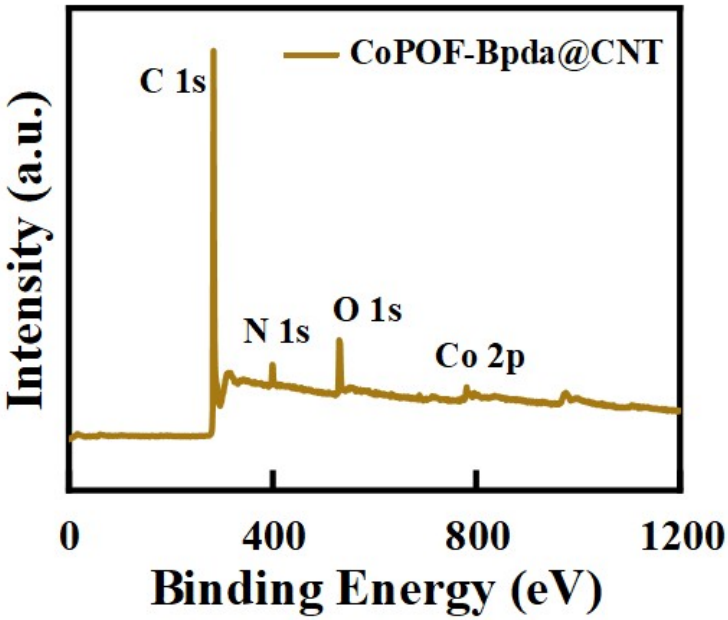

Fig. S13. XPS spectrum of CoPOF-Bpda@CNT.

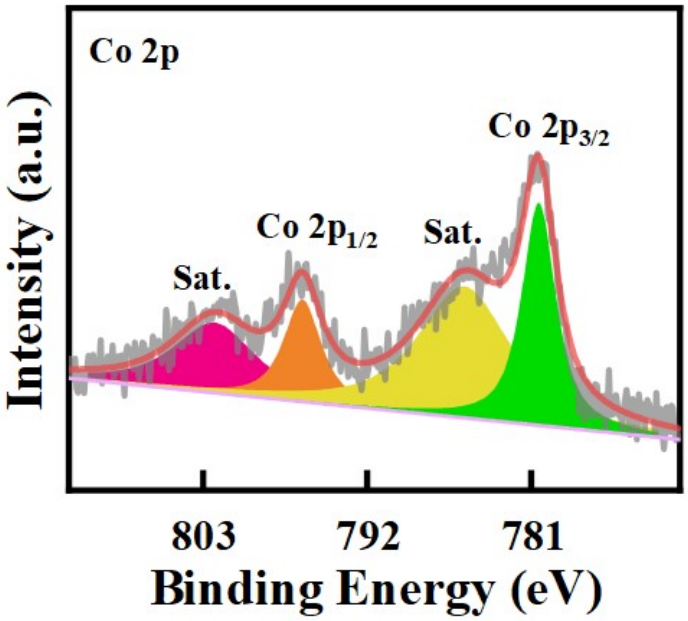

Fig. S14. Co 2p XPS spectrum of CoPOF-Bpda@CNT.

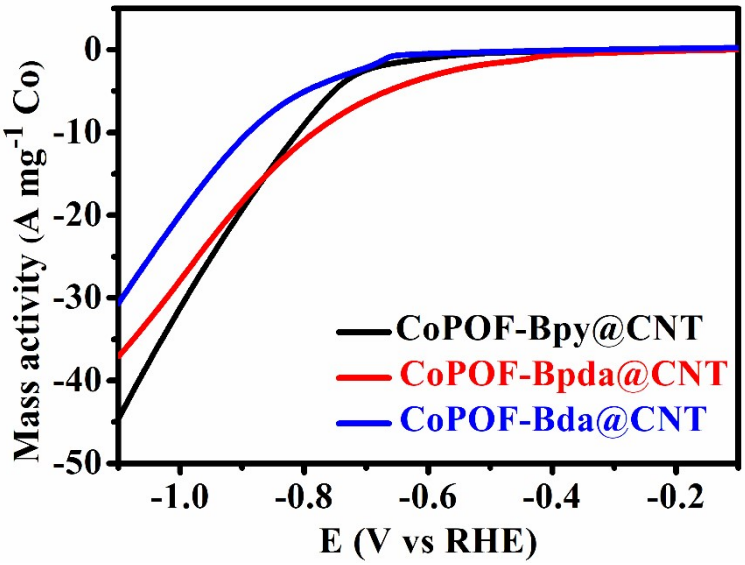

Fig. S15. Mass activities of CoPOF-Bpy@CNT CoPOF-Bda@CNT, and CoPOF-Bpda@CNT by normalizing the current densities with respect to the Co contents.

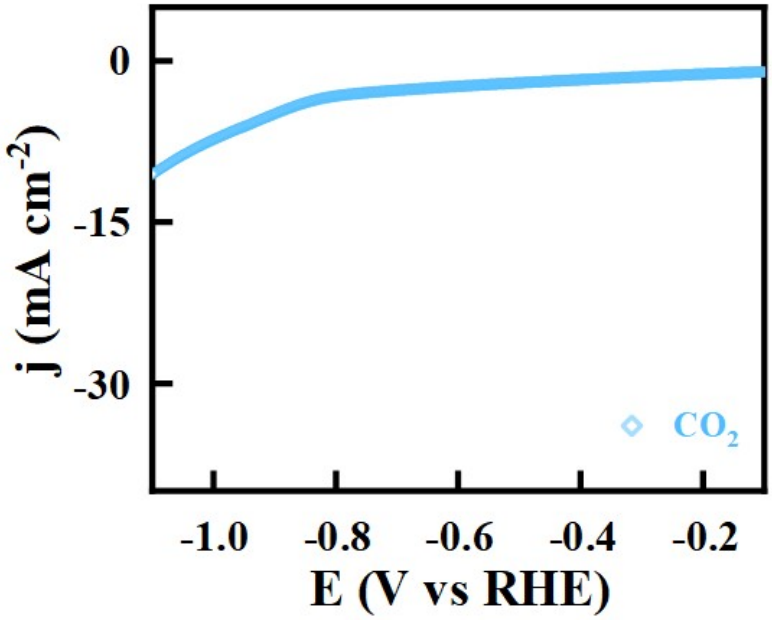

Fig. S16. LSV plot of pure CNTs in a CO_2-saturated $KHCO_3$ solution.

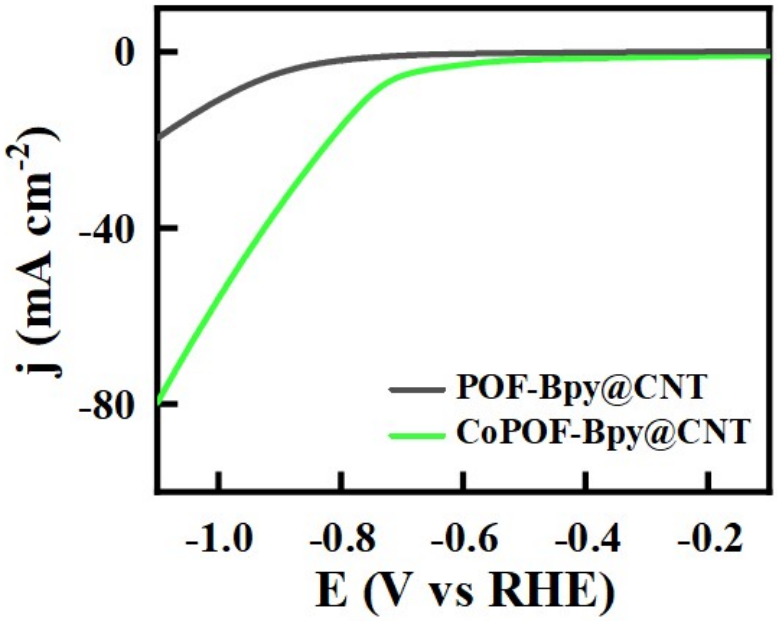

Fig. S17. LSV plots of CoPOF-Bpy@CNT and POF-Bpy@CNT in a CO_2-saturated $KHCO_3$ solution.

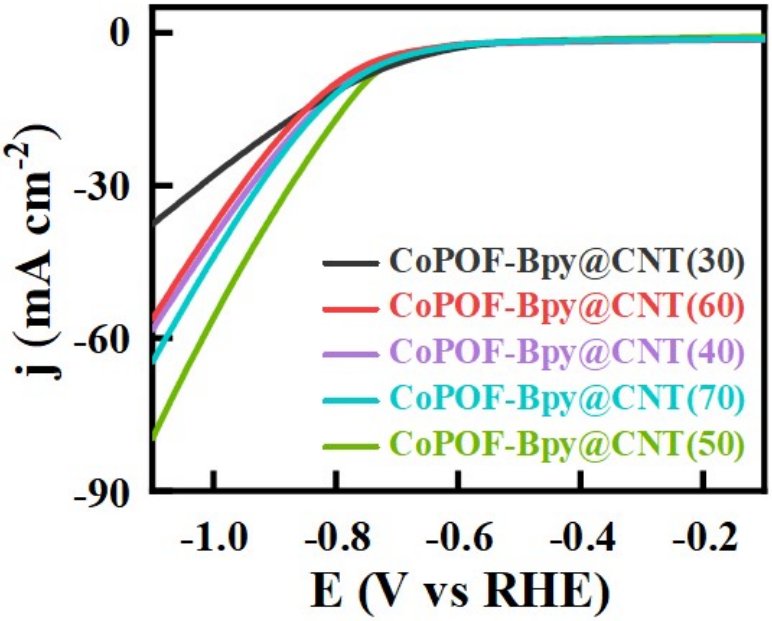

Fig. S18. LSV plots of CoPOF-Bpy@CNT(X) in a CO_2-saturated $KHCO_3$ solution.

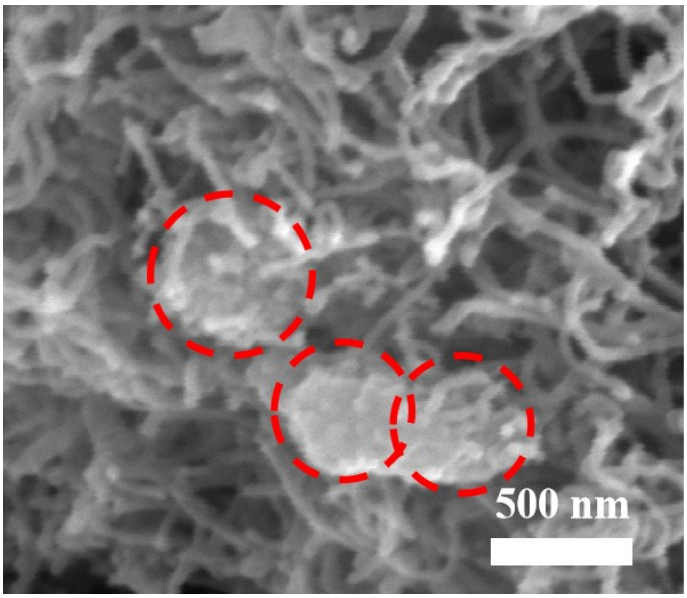

Fig. S19. SEM image of CoPOF-Bpy@CNT(30).

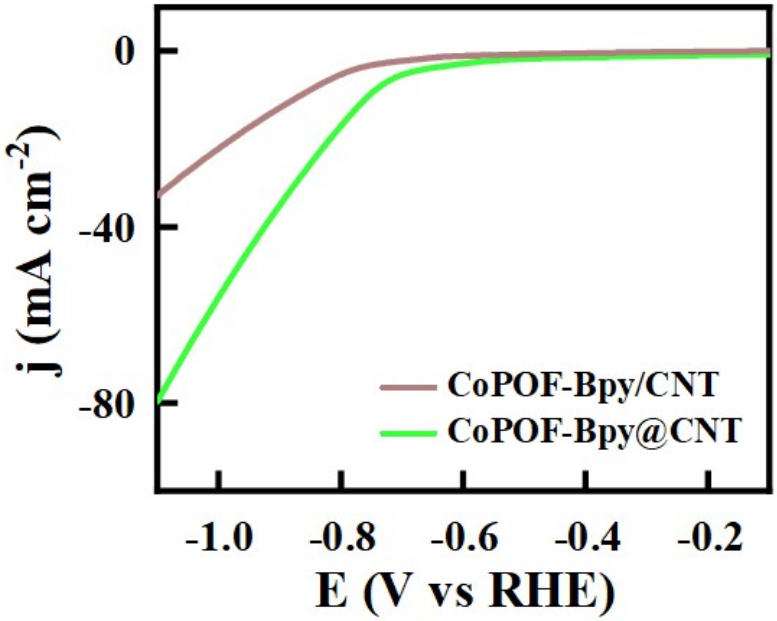

Fig. S20. LSV plots of CoPOF-Bpy@CNT and CoPOF-Bpy/CNT in a CO_2-saturated $KHCO_3$ solution.

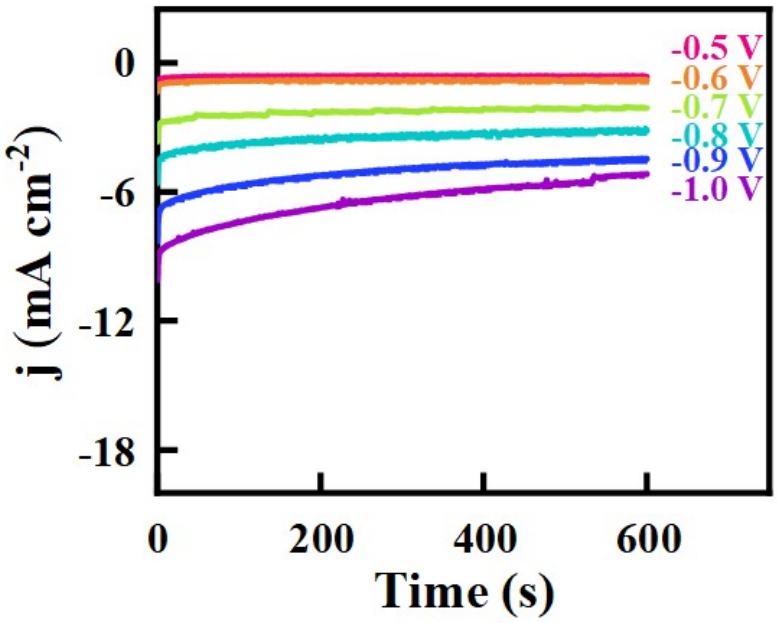

Fig. S21. Time-dependent total catalytic current densities (j_{total} ~ t) of CoPOF-Bda@CNT in a wide potential range from –0.5 V to –1.0 V vs RHE.

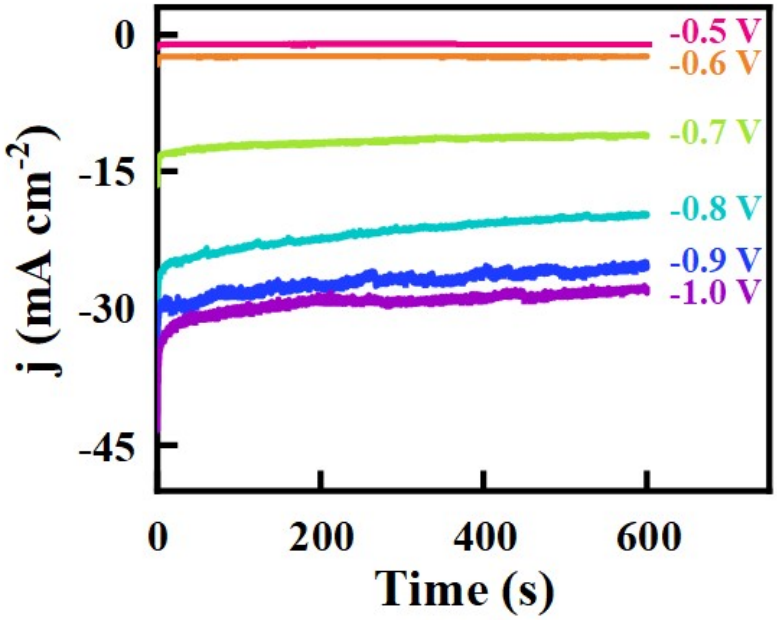

Fig. S22. Time-dependent total catalytic current densities (j_{total} ~ t) of CoPOF-Bpda@CNT in a wide potential range from –0.5 V to –1.0 V vs RHE.

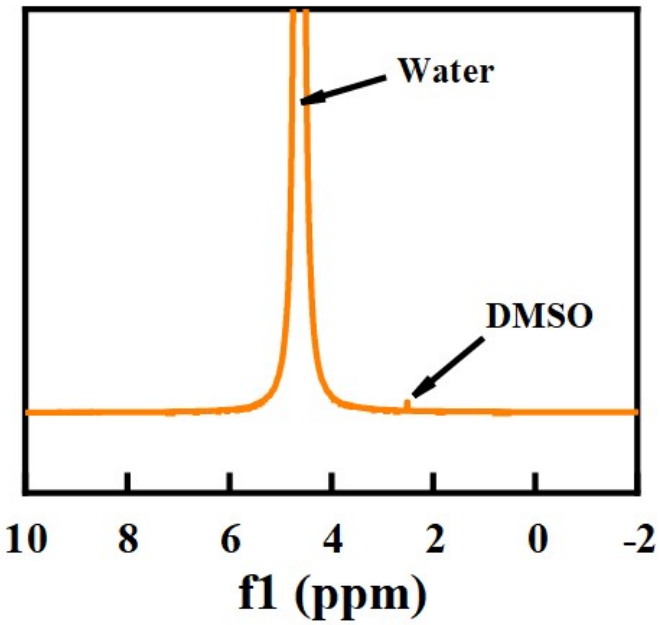

Fig. S23. ^{1}H NMR spectrum of liquid product after long-term CO_2RR for CoPOF-Bpy@CNT at –0.7 V vs RHE in CO_2-saturated 0.5 M $KHCO_3$ solution.

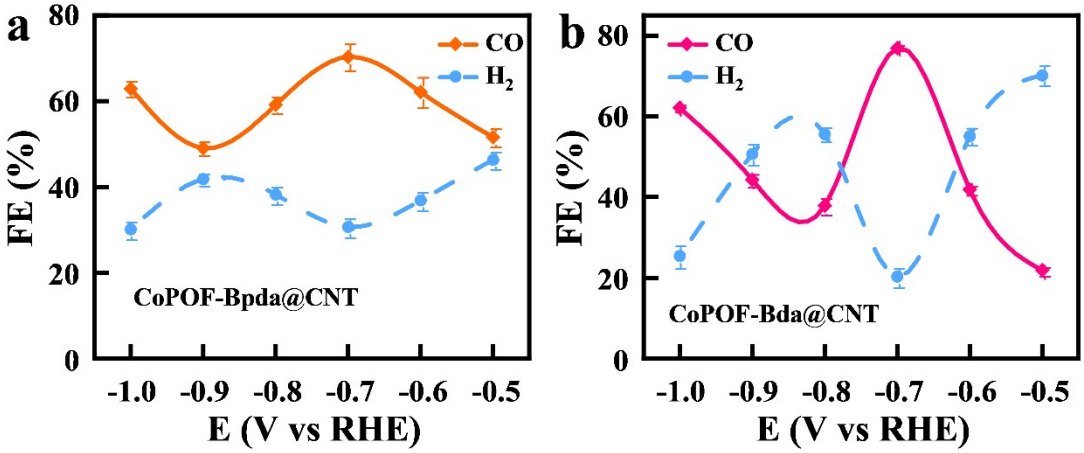

Fig. S24. FE_{CO} and FE_{H2} of (a) CoPOF-Bpda@CNT and (b) CoPOF-Bda@CNT at different applied potentials.

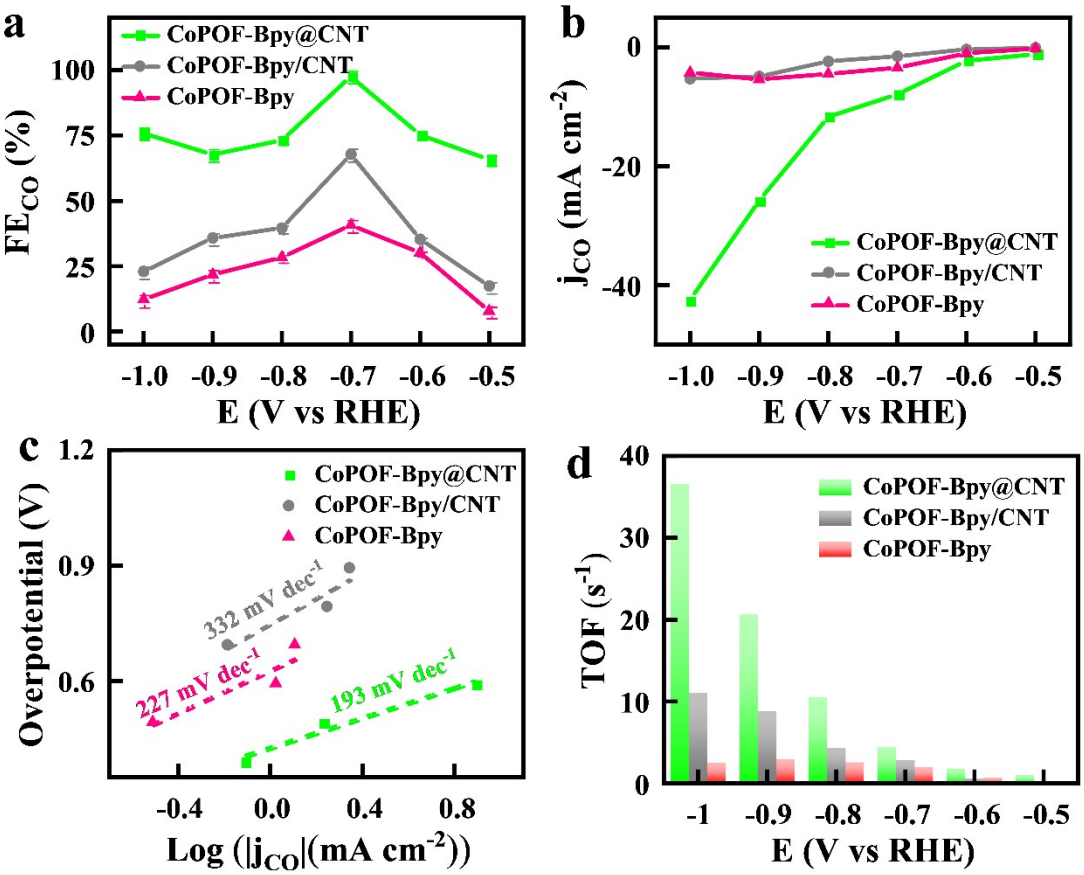

Fig. S25. (a) FE_{CO} of CoPOF-Bpy@CNT, CoPOF-Bpy, and CoPOF-Bpy/CNT at different applied potentials; (b) Partial current densities of CO, (c) Tafel plots, and (d) TOF values of CoPOF-Bpy@CNT, CoPOF-Bpy, and CoPOF-Bpy/CNT.

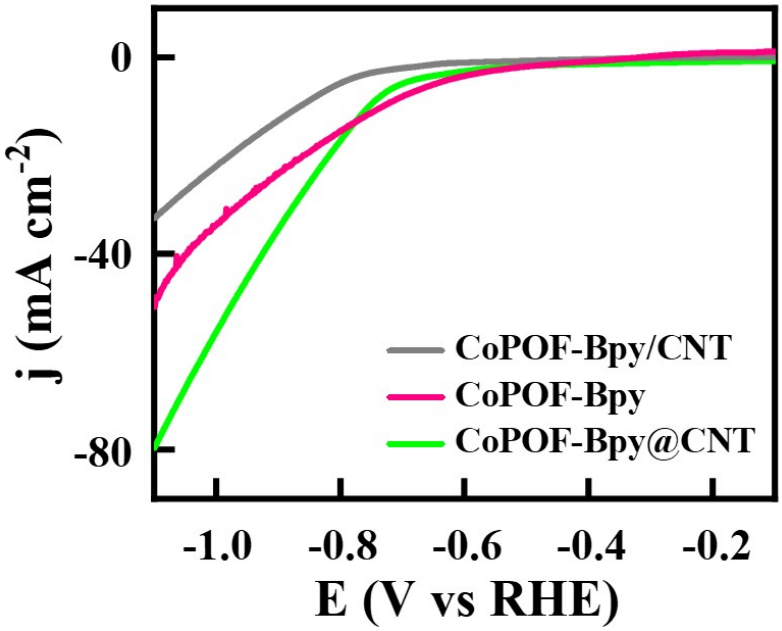

Fig. S26. LSV plots of CoPOF-Bpy@CNT, CoPOF-Bpy, and CoPOF-Bpy/CNT in a CO_2-saturated 0.5 M $KHCO_3$ solution.

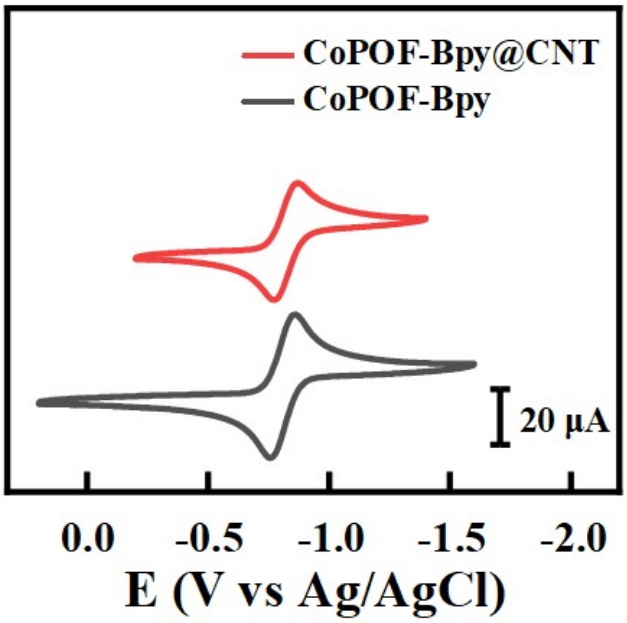

Fig. S27. CV plots of CoPOF-Bpy@CNT and CoPOF-Bpy in a 0.1 M NBu_4PF_6/DMF solution under nitrogen atmosphere with a scan rate of 100 mV s^{-1}.

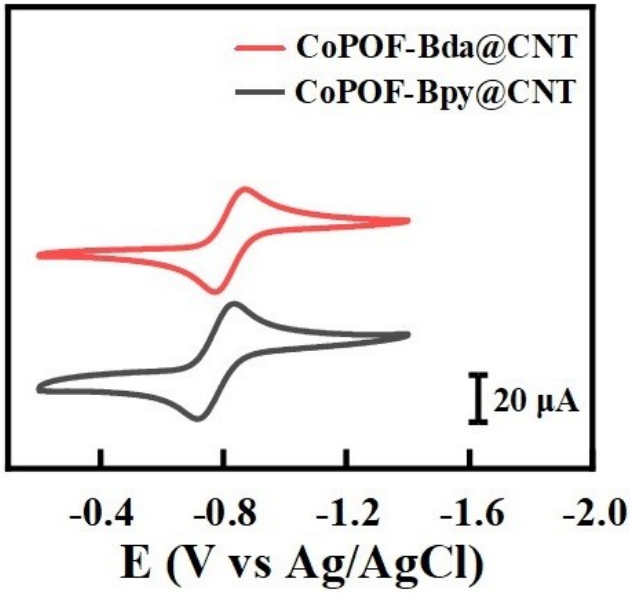

Fig. S28. CV plots of CoPOF-Bpy@CNT and CoPOF-Bda@CNT in a 0.1 M NBu_4PF_6/DMF solution under nitrogen atmosphere with a scan rate of 100 mV s^{-1}.

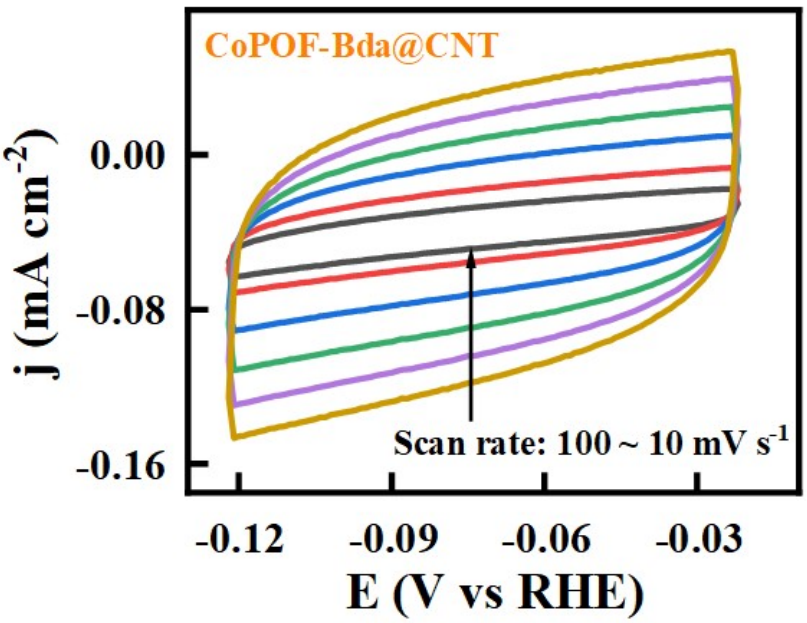

Fig. S29. CV plots of CoPOF-Bda@CNT in the non-Faradaic region with various scan rates (10 ~ 100 mV s^{-1}).

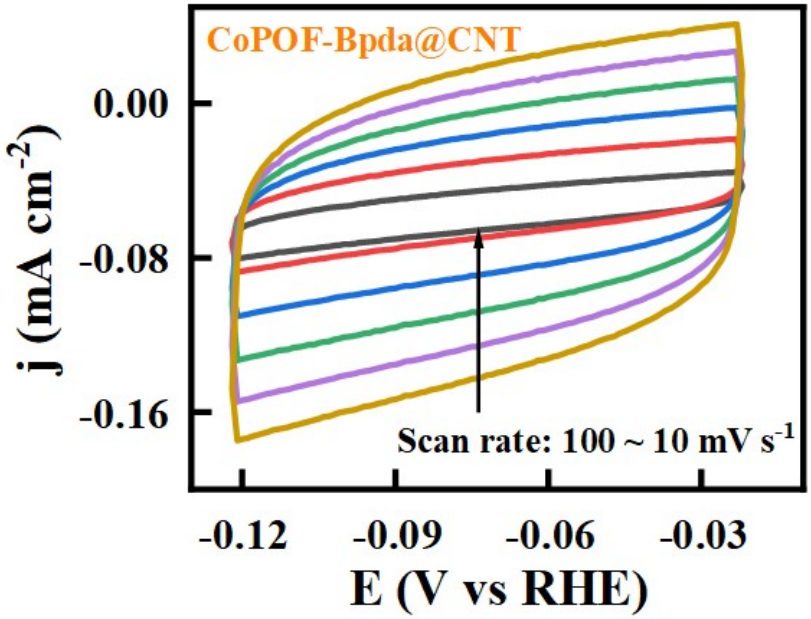

Fig. S30. CV plots of CoPOF-Bpda@CNT in the non-Faradaic region with various scan rates (10 ~ 100 mV s^{-1}).

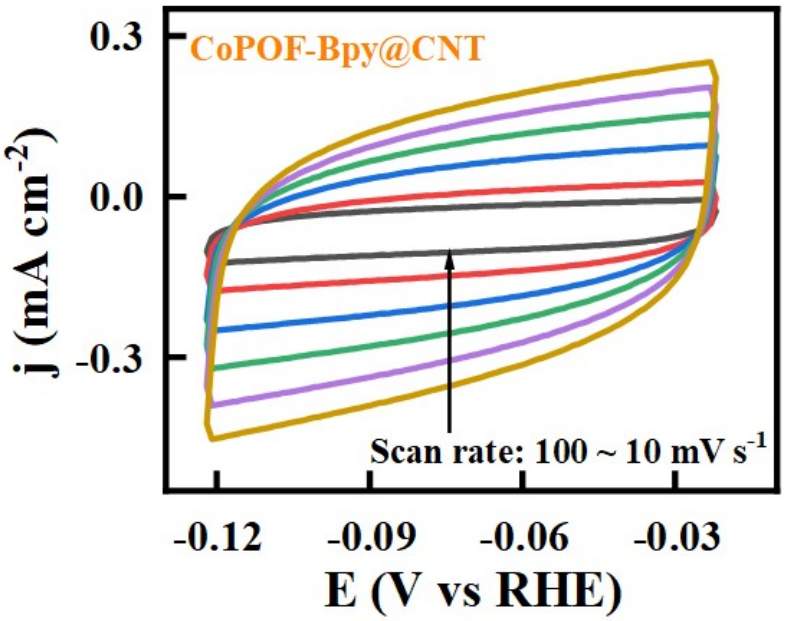

Fig. S31. CV plots of CoPOF-Bpy@CNT in the non-Faradaic region with various scan rates (10 ~ 100 mV s^{-1}).

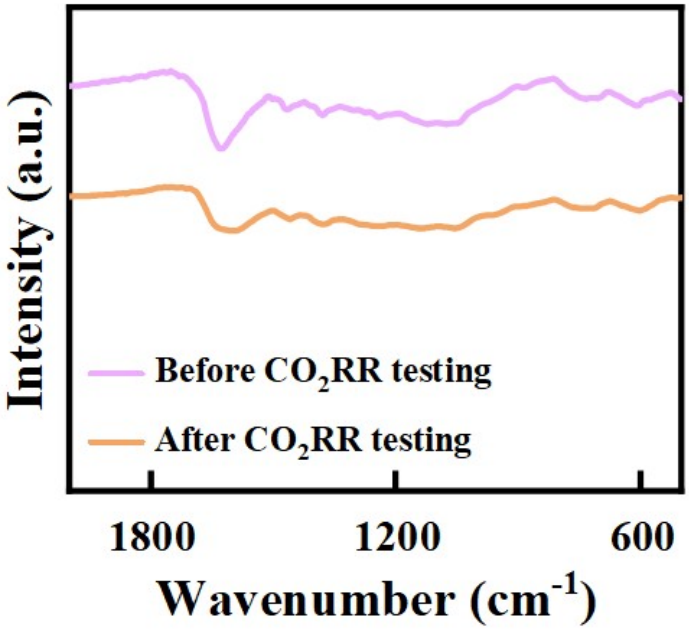

Fig. S32. The comparison of FT-IR spectra of CoPOF-Bpy@CNT before and after long-term CO_2RR.

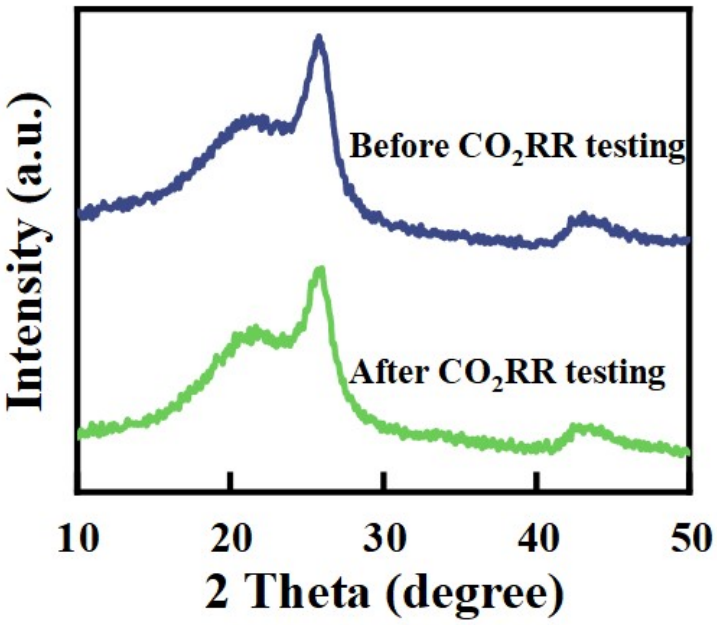

Fig. S33. The comparison of XRD patterns of CoPOF-Bpy@CNT before and after long-term CO_2RR.

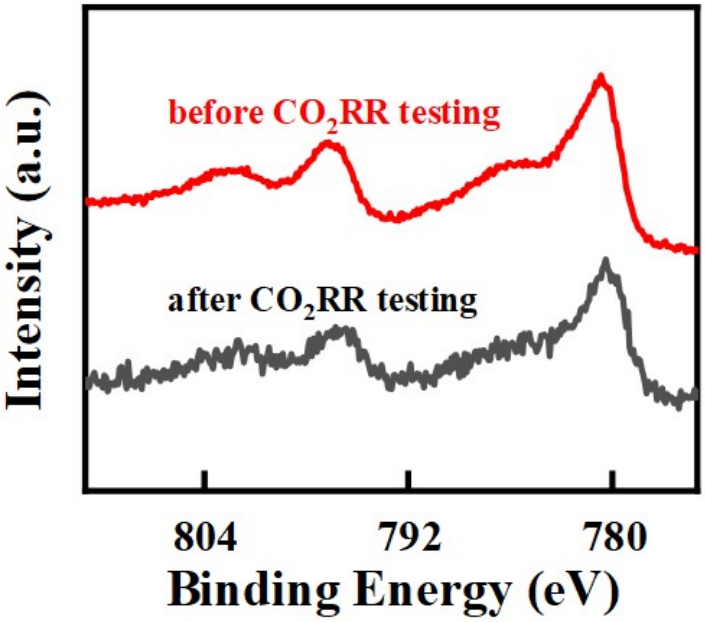

Fig. S34. The comparison of Co 2p XPS spectra of CoPOF-Bpy@CNT before and after long-term CO_2RR.

Table S2 Comparison of the electrocatalytic CO_2RR performance of recently reported CoPor-based POFs electrocatalysts.

Catalysts	Electrolyte	V vs. RHE	FE_{CO} / %	j_{CO} / mA cm^{-2}	TOF / s^{-1}	Ref.
CoPOF-Bpy@CNT			97.5	7.9	36.6 at –1.0 V	
CoPOF-Bpda@CNT	0.5 M $KHCO_3$	–0.7	70.3	5.7	26 at –1.0 V	This work
CoPOF-Bda@CNT			76.8	1.6	13.7 at –1.0 V	
COF-367-Co	0.5 M $KHCO_3$	–0.67	90	3.3	0.53	1
COF-367-Co(1%)			90	0.45	2.6	
COF-366-Co@CNT			92	6.8	/	
COF-366-$(OMe)_2$-Co@CNT	0.5 M $KHCO_3$	–0.68	94	7.3	11877 h^{-1} at –0.77 V	2
COF-366-$(OH)_2$-Co@CNT			90	6.0	/	
COF-366-$(F)_4$-Co@CNT			91	5.7	/	
CoCoPCP	0.5 M $KHCO_3$	–0.55	82	1.5	0.9	3
CoCoPCP/CNTs			94	8.1	2.4	
MWCNT-Por-COF-Co	0.5 M $KHCO_3$	–0.6	99.3	18.77 at –1.0 V	72 at –1.0 V	4
CoP@CNT			98		2.2	
CoP-Ph@CNT	0.5 M $KHCO_3$	–0.57	82	/	0.9	5
CoP-F@CNT			12		0.1	

References

1. S. Lin, C. S. Diercks, Y.-B. Zhang, N. Kornienko, E. M. Nichols, Y. Zhao, A. R. Paris, D. Kim, P. Yang, O. M. Yaghi and C. J. Chang, Covalent organic frameworks comprising cobalt porphyrins for catalytic CO_2 reduction in water, *Science*, 2015, **349**, 1208–1203.
2. Y. Lu, J. Zhang, W. Wei, D.-D. Ma, X.-T. Wu and Q.-L. Zhu, Efficient carbon dioxide electroreduction over ultrathin covalent organic framework nanolayers with isolated cobalt porphyrin units, *ACS Appl. Mater. Interfaces*, 2020, **12**, 37986–37992.
3. T. Wang, L. Xu, Z. Chen, L. Guo, Y. Zhang, R. Li and T. Peng, Central site regulation of cobalt porphyrin conjugated polymer to give highly active and selective CO_2 reduction to CO in aqueous solution, *Appl. Catal. B*, 2021, **291**, 120128.
4. H. Dong, M. Lu, Y. Wang, H.-L. Tang, D. Wu, X. Sun and F.-M. Zhang, Covalently anchoring covalent organic framework on carbon nanotubes for highly efficient electrocatalytic CO_2 reduction, *Appl. Catal. B*, 2022, **303**, 120897.
5. Y. Wang, X.-P. Zhang, H. Lei, K. Guo, G. Xu, L. Xie, X. Li, W. Zhang, U.-P. Apfel and R. Cao, Tuning electronic structures of covalent Co porphyrin

polymers for electrocatalytic CO_2 reduction in aqueous solution, *CCS Chem.*, 2022, **4**, 2959–2967.